Integrity of arousal-regulating brain circuitry predicts human cognitive abilities

Authors: Ella Podvalny, Ruben Sanchez-Romero, Michael W. Cole

Arousal state is regulated by the brainstem nucleus locus coeruleus, which sends wide-reaching projections to cortex. How this powerful neuromodulatory system is recruited to aid cognition is largely underexplored. Here, we hypothesized that select cortical regions may activate the arousal system, which in turn modulates large-scale brain activity, creating a circuit whose integrity predicts cognitive ability. We utilized the Human Connectome Project 7T functional magnetic resonance imaging dataset (N=149), acquired at rest with simultaneous eye tracking, along with extensive cognitive assessment for each subject. First, we discovered select frontoparietal cortical regions that likely drive large-scale spontaneous brain activity specifically via engaging the arousal system. Second, we show that the integrity of the arousal circuit driven by bilateral posterior cingulate cortex (associated with the default mode network) predicts subjects' cognitive abilities. This suggests that a cortical region that is typically associated with self-referential processing supports cognition by regulating the arousal system.

Keywords: *arousal; spontaneous brain activity; posterior cingulate cortex; default mode network; cognition; resting state*

INTRODUCTION

Cognition is greatly influenced by ongoing fluctuations in arousal[1–3]. Consider a student at a test – to perform well, they need to either increase their level of arousal, if they feel tired, or decrease it, if they feel stressed. In this case, the task – performing well on a test – defines the optimal level of arousal, whereas a student's ability to adeptly shift their arousal level allows strategic control of behavioral attributes: for example, balancing the exploration-exploitation trade-off or adjusting reaction times[4–6]. Accordingly, several scholars have theorized that arousal-related processes play a major role in general intelligence[7] and creativity[8], whereas an inability to appropriately adjust arousal may severely compromise social, emotional, and cognitive aspirations[9]. Despite these crucial roles of top-down arousal control in human behavior, the possible arousal-regulating cortical circuits and their effect on general cognitive abilities remain poorly understood.

The arousal state is modulated by brainstem locus coeruleus (LC) neurons, whose axon terminals extend throughout the entire cortex via extensive branching, releasing mostly norepinephrine (NE) and some dopamine (DA)[10–12]. While evidence for LC receiving inputs back from cortex in humans is still inconclusive[13], previous research points to the importance of investigating such a possibility. Electrical stimulation of dorsomedial prefrontal cortex (dmPFC) in rats, for example, results in increased LC firing, whereas chemical inactivation results in inhibition[14,15]. In humans, Granger causality analysis of fMRI signals suggests a directional effect of posterior inferior parietal lobule (pIPL), a DMN (default mode network) region, on the arousal system[16]. These findings point to a strong possibility of cortical neurons projecting to LC and potentially controlling its functionality.

While fMRI is often considered too sluggish to identify directional relations, tonic (resting state) neuromodulatory effects of noradrenergic projections are known to occur at a timescale slow enough to be detected and distinguished from fast glutamatergic effects of cortical projections. First, NE receptors are metabotropic – that is, requiring multiple metabolic steps for activation, which may take hundreds of milliseconds to minutes. This may explain the findings that extracellular NE in cortex,

due to either tonic LC firing or direct application, results in only sluggish (seconds to minutes) effect on spontaneous brain activity in animals[17], and the recovery from the effects of NE application in rat cortex takes up to a minute[18]. Second, noradrenergic axons lack myelin and exhibit variable conduction velocity[2,19], thus target cortical cells are triggered with low temporal precision by slow tonic LC activity at resting state (1-6Hz)[20,21]. These slow timescales are very likely within the detection range of fMRI with a temporal resolution of 1 Hz.

In addition, the distinct neurobiology of ascending and descending projections to LC predicts a likely opposing functional connectivity during resting state. First, NE is considered a modulator of a neural gain – that is, it may contribute to both the suppression of spontaneous baseline activity and to the increase of relative stimulus-triggered activity[3,22]. This is consistent with previous studies that show suppressive effects of pupil-linked arousal in human cortex[16], and a decrease in spontaneous firing due to application of NE in rat cortex [17,18,23]. Further, because cortical long-range projections are mostly excitatory, a positive effect of cortical firing on LC is expected (Figure 1). Crucially, because it is unclear to what extent animal models have sufficient top-down control of the arousal state, using fMRI in healthy human volunteers to test the hypothesis of bi-directional connectivity between cortical activity and the arousal state is our best option at this time.

Here, we aim to: (1) identify the cortical regions that exert top-down regulation of the arousal state (pupil size) and cause a subsequent large-scale activity modulation, (2) test whether the arousal-related circuit-level connectivity of each candidate region predicts individual differences in cognitive performance. To achieve these aims, we use a 7T fMRI dataset provided by the Human Connectome Project, which includes prolonged resting state fMRI recordings in a substantial number of subjects who also underwent extensive cognitive testing, allowing us to test the relationship between individual brain connectivity measures and behavioral performance.

RESULTS

Our first goal was to identify cortical regions that are likely to regulate the arousal system (Fig.1). We reasoned that activity in such regions must satisfy (at least) the following conditions:

- **(i)** Directional effect: Brain activity in cortical arousal-driver regions must be positively correlated with an indicator of arousal (pupil size) since the long-range projections from cortex to LC are more likely to be excitatory (see *Introduction* above for details) (Fig. 1);
- **(ii)** Independent effect: it is possible that two cortical regions, A and B, predict the arousal signal, while in fact only region A is connected to LC whereas region B is merely connected to A. For this reason, to determine the effects of cortical activity on the arousal signal, we need to account for correlations among cortical regions.
- **(iii)** Circuit-level effect: It must be demonstrated that the arousal driver regions induce delayed negative effects on spontaneous brain activity (due to NE-linked suppression) that are specifically *mediated* by the arousal signal (i.e., cannot be fully explained by direct cortical-cortical connections).

While it is theoretically possible that the above procedure will misidentify cortical regions that are affected by activity from regions we do not measure ("unmeasured confounders"), this is unlikely with the full brain coverage of fMRI. It is also likely that additional cortical regions that suppress the arousal system via the generally rare long-range inhibitory projections or by targeting inhibitory interneurons within LC exist in the brain. However, we do not test for such a hypothesis herein since such anatomically fine-grained effects are difficult to discern with fMRI, where each voxel contains hundreds of thousands of neurons.

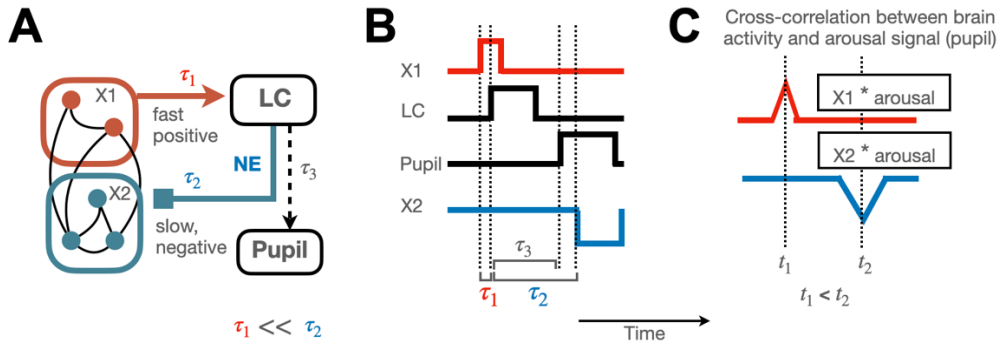

Figure 1. Hypothesized large-scale circuit regulating tonic arousal, based on temporal lag and sign of time series correlations. A. Simplified wiring diagram of a large-scale brain circuit for recruitment of the brainstem arousal system. Select cortical regions (X1) signal LC via fast myelinated projections (with τ_1 signifying temporal delay), whereas LC activation leads to slow NE release in cortex, which in turn modulates cortical sustained activity (with a delay of τ_2). In resting state, NE release suppresses spontaneous brain activity. Non-light-mediated pupil size fluctuations reflect LC activity at rest (with a delay of τ_3). **B.** Neural activity cascade expected from circuit depicted in A during resting state. Cortical regions X1 cause increase in LC tonic activity. X1 regions may also cause network-level activation in regions X2 (not depicted). LC tonic firing in turn results in large-scale slow release of NE, resulting in a decrease of cortical spontaneous activity with a delay of multiple seconds. **C.** Expected cross-correlation (a measure of signal similarity as a function of temporal lag) between X1/X2 type of brain regions and the arousal signal, whereas t_1 and t_2 depict the relative timing of the cross-correlation peaks/troughs. Positive peaks are expected to appear earlier than negative troughs ($t_1 < t_2$), irrespective of whether the pupil size or LC activity is used to indicate the arousal state.

Select cortical regions exhibit the properties of arousal regulation

To identify the potential arousal driving regions we used 7T fMRI HCP data recorded at 1 Hz temporal resolution during resting state with concurrent eye tracking (see Methods). We opted to using the pupil size as the arousal signal rather than LC activity since the signal acquisition methodology was not specifically optimized for LC in the HCP dataset, and non-light-mediated ongoing fluctuations of pupil size have been shown to reflect resting state electrophysiological LC activity with temporal precision higher than that of hemodynamic response.

We first examine the cross-correlation between fMRI BOLD signal and pupil size for each brain region (Figure 2A-B). The results include positive correlations between multiple brain regions and pupil size, at a negative time lag (i.e., brain activity precedes the change in pupil size), and thus satisfying the first criterion for arousal-driving regions ("directional effect"). Note that the regions positively correlated with pupil size are situated mostly in frontal and parietal brain regions belonging to default mode network (DMN), frontoparietal network (FPN) and cingulo-opercular network (CON) (Figure 2A-B, supplemental figure 2 or figure 2E for network partition). The positive correlation peak appears significantly earlier than the correlation trough (Figure 2B, 2D), which dominates the brain networks specializing in motor responses and processing of sensory stimuli (e.g., Vis2, SMN). Such negative correlations are consistent with NE-driven inhibition of spontaneous activity and the localization in motor and sensory networks is expected due to higher density of alpha 1A and alpha 2A noradrenergic receptors in these two networks[24]. Further, this result is consistent with the possibility of suppression of spontaneous brain activity due to increase in neural gain (Figure 2C) and with previously reported correlations with pupil size that were positive in DMN and negative in visual brain areas[16].

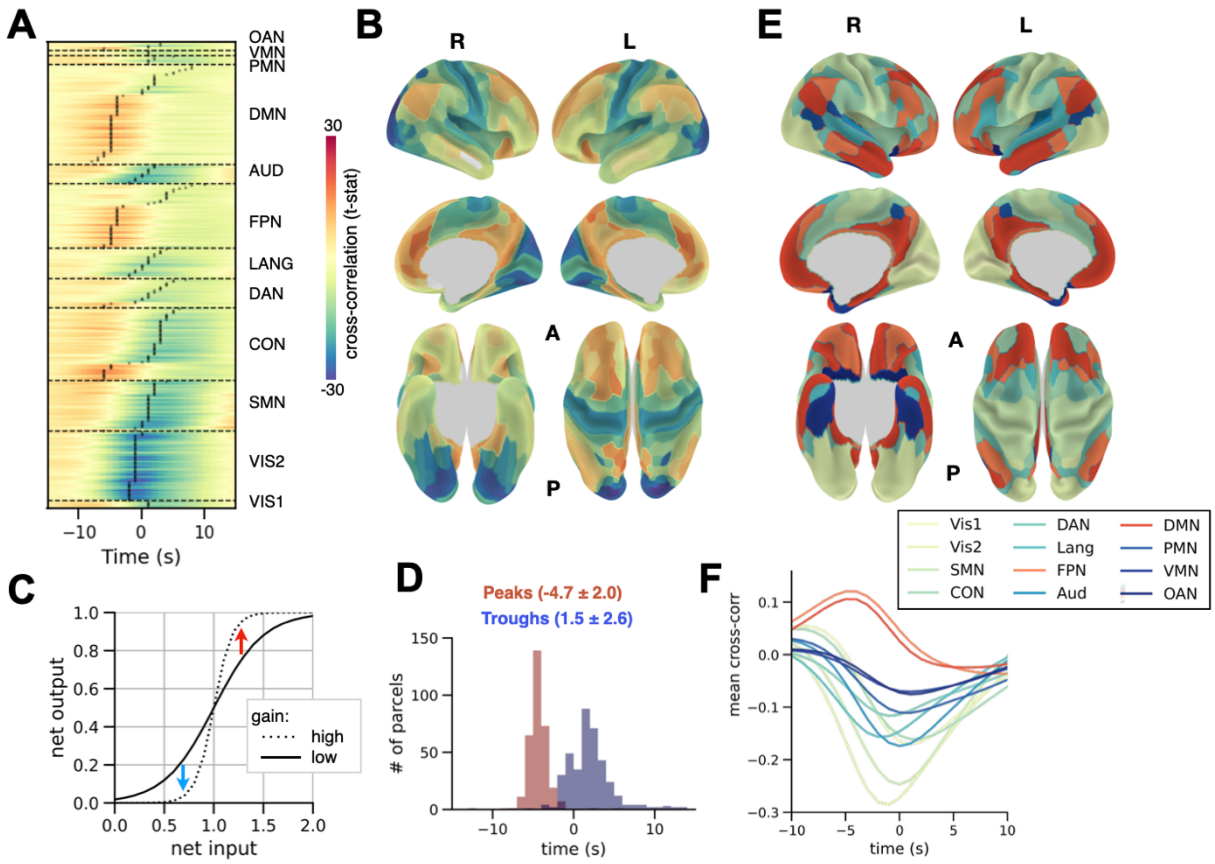

Figure 2. Spatiotemporal interactive dynamics of arousal state and spontaneous brain activity. A. Cross-correlation between pupil size predictor and fMRI cortical parcel-level activity (Glasser parcellation) compared with a null distribution calculated via reversal of pupil size time course (t-statistic). The parcels are grouped according to large-scale resting-state brain networks [25] and sorted according to peak/trough time lag (black dots). **B.** Peaks/trough amplitude of pupil-brain cross-correlation (same color scale as A) presented on the cortical surface. **C.** Illustration of gain modulation depicting the potential suppression of low brain activity such as during resting state (blue arrow) and amplification of high brain activity (red arrow). **D.** Distribution of cross-correlation peak/trough time lags across brain regions. **E.** Large-scale resting-state networks presented on the cortical surface. **F.** Averaged cross-correlation between pupil size and brain activity within each resting-state network (Vis1:Visual 1, Vis2: Visual 2, SMN:somatomotor, CON:cingulo-opercular, DAN:dorsal attention, Lang:language, FPN: frontoparietal, Aud:Auditory, DMN: default mode, PMN:posterior multimodal, VMN: ventral multimodal, OAN: orbito-affective). Networks that on average show larger absolute value of positive peak than negative trough are colored in warm colors (FPN and DMN), same color code as (**E**).

The positive cross-correlation between region-level brain activity and pupil size could either reflect arousal-driving cortical regions or merely reflect propagation of activity within cortical resting state networks without causally affecting the arousal state (see criterion (ii)). To discern between these two possibilities, we constructed a two-step model that progressively eliminated cortical regions that lost the effect on arousal due to cross-region correlation (see Methods). In the first step, we construct a model for each resting state network to test the effect of each candidate brain region on the arousal state while including all other regions within the same network as covariates. In the second step, we combine all regions that show significant effects in the multiple models of the first step to account for possible cross-networks correlations (see Methods, Equation 1). As expected, this method eliminated most cortical brain regions that showed a positive effect on the arousal state regardless of network-level correlations

(compliant with criterion (i), Figure 2B) and only the regions that showed significant *independent* effects on arousal state remained (compliant with criterion (ii), presented in Figure 3A).

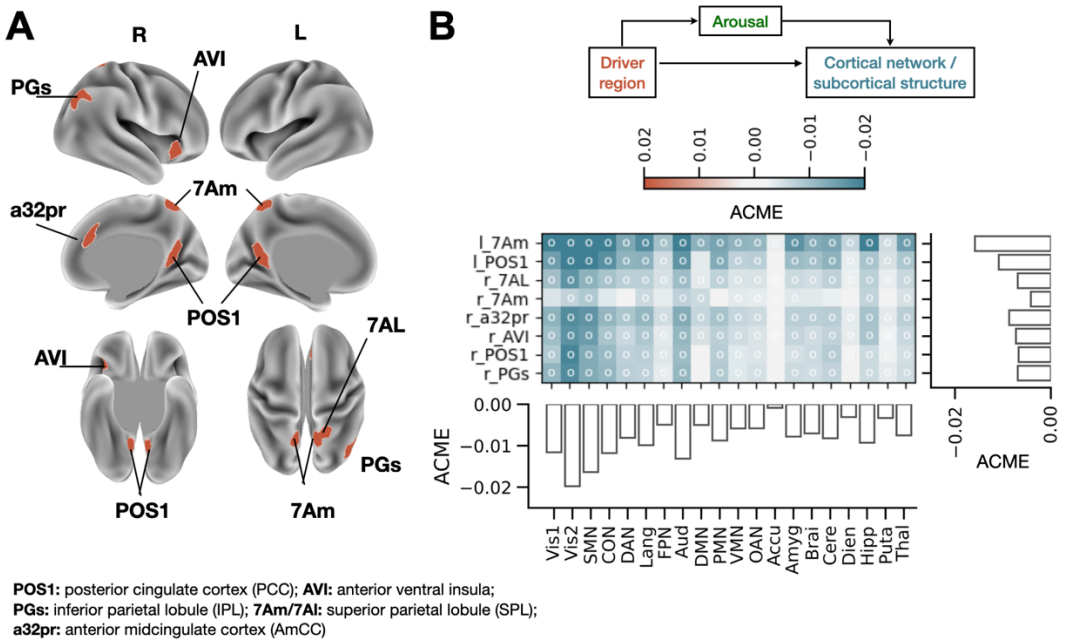

Figure 3. Regions identified as regulating large-scale spontaneous activity via pupil-linked arousal. A. Brain regions (Glasser parcellation) predictive of pupil-linked arousal in agreement with "independent effect" criterion. These regions were identified by considering network-level and cross-network activity correlations via multiple regression linear mixed models. The legend provides commonly used names for Glasser brain regions. **B.** Effects of brain regions presented in A on large-scale network and subcortical activity as mediated by arousal. **Top:** illustration of causal mediation analysis conducted for each region presented in A. **Bottom:** Each cell of the matrix shows ACME (Average Causal Mediation Effect), representing the level of influence of brain activity in the arousal-driver region on subsequent activity in the cortical network or subcortical structure that is specifically routed via arousal. The white circles indicate p-value < 0.05 (FDR corrected). The bar plots show the ACME averaged across the arousal-driver regions (horizontal bars) and across the arousal-driven networks/subcortical areas (vertical bars). The network abbreviation is the same as Figure 2.

The candidate arousal-driver regions identified (Figure 3A) include: (1) bilateral POS1 (posterior-occipital sulcus 1), regions residing within the posterior cingulate cortex (PCC); (2) bilateral 7Am (7 anterior-medial), regions in superior parietal lobule located on the medial side; (3) right 7AL (7 anterior-lateral), found also in superior parietal lobule on the lateral side; (4) PGs (parietal area G superior) – area in the angular gyrus of inferior parietal lobule (IPL); (5) a32pr (anterior 32 prime), a region in anterior midcingulate cortex; and (6) AVI, anterior ventral insular area.

To test whether these candidate arousal-driver regions (Figure 3A) indeed invoke large-scale activity modulation via the arousal system (criterion (iii)), we conducted a causal mediation analysis. Namely, we used linear mixed effect models testing the effect of each driver region on brain-wide activity via arousal state (pupil size) while the potential direct effect (bypassing arousal) is accounted for (Figure 3B top, see Methods, Equations 2-3) (Figure 3B). According to our hypothesis, we expect to see a negative mediation effect because the arousal driver regions should induce inhibition of spontaneous brain activity via the arousal system. This analysis revealed that all candidate arousal-driver regions showed significant mediation effects (figure 3B bottom, FDR corrected for multiple comparisons). Note the regions of left superior parietal lobule (left 7Am) and PCC (POS1) showed the strongest effects, suggesting these regions may play an especially prominent role in regulating widespread cortical activity via the arousal system.

Large-scale arousal circuit connectivity predicts individual cognitive performance

In a final analysis, we tested the hypothesis that the integrity of the identified large-scale arousal-regulating circuits predicts individual differences in cognitive performance. This hypothesis stems from the idea that each cognitive task requires an arousal level that is optimal for that specific task; thus, an adaptive arousal-regulating circuit should improve general cognitive ability rather than one specific task. To this end, we calculated the cognitive ability score for each participant as an aggregate performance metric across cognitive tasks (see Methods, Figure 4A). Next, we fit a mediation model for each individual subject (see Methods) to estimate the subject-level average causal mediation effect (ACME) for each arousal-driving and arousal-affected brain area. The distribution of ACME averaged across brain regions is depicted in Figure 4B. The negative values of ACME signify arousal-driven suppression of spontaneous brain activity. The relationship between global ACME and individual cognitive ability was negative (coef. = -27.5, p-value = 0.043, Figure 4D).

Previous research has shown that both LC integrity[26] and cognitive performance[27] decline with age. In our data, the participants' age was between 22 and 36 (Figure 4C), and the effect of age on cognitive ability, while not statistically significant (coef. = -0.05, p-value = 0.07, Figure 4E), is consistent with the previous findings.

Because we identified brain regions that independently drive the arousal state, we are especially interested in testing which region-specific arousal-related circuits predict cognitive ability. To this end, since arousal-driven suppression of spontaneous brain activity is global, for each arousal driver region we averaged the causal mediation effect across the brain (Figure 3B, right horizontal bars). Next, we tested whether this effect (ACME), signifying arousal-circuit integrity, predicted cognitive ability. We also included age as a covariate and as an interaction term with ACME in our next model (Methods, Equation 6).

Individual-subject scores of cognitive ability were significantly predicted by the circuit-level connectivity of right (coef. = -3.8, p-value = 0.003, FDR-corrected) and left (coef. = -2.4, p-value = 0.021) POS1 (PCC) only (Figure 4F). The effect was negative, indicating that stronger arousal-linked control by PCC predicts a higher cognitive ability score (since the mediation effect gets stronger in the negative direction). The effect of age on cognitive ability scores was negative, which is consistent with prior literature, but again not significant (p-value > 0.05) in the relatively narrow age group that was included in the present study. We also detected a positive interaction effect with age in the bilateral POS1 (coef = 0.12, pval =0.004 and coef = 0.08, pval =0.03) (Figure 4A, bottom panel), indicating that the effect of the arousal circuit integrity on cognitive performance gets weaker with age.

Finally, as a control analysis, we tested whether the effects above were, as hypothesized, due to mediation or were rather due to individual pathways from driver regions to arousal or from arousal to the rest of the brain (see Methods, Equations 7 and 8 correspondingly). Models of individual pathways did not produce any significant effects on behavior (all p>0.05 after FDR correction).

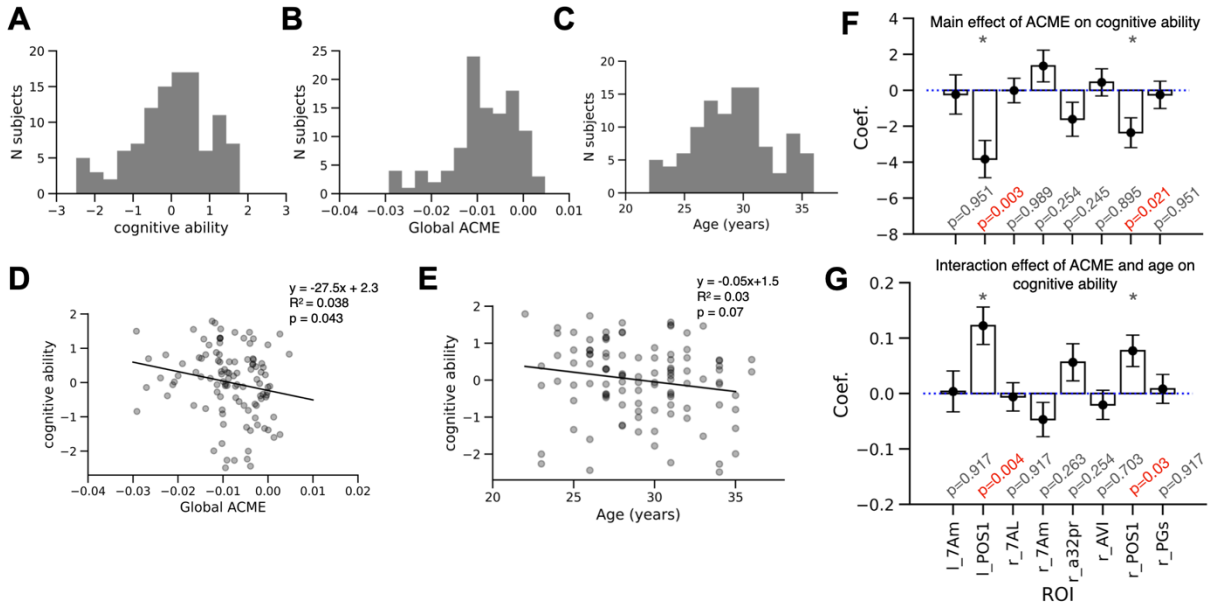

Figure 4. Integrity of arousal-regulating brain circuit predicts individual differences in cognitive ability. A. Distribution of cognitive ability scores across subjects. **B.** Distribution of global ACME (Averaged Causal Mediation Effect), that is, ACME averaged across the driving and the affected brain areas. **C.** Distribution of age across subjects. **D.** The relationship between global ACME and cognitive ability with linear model fit result depicted and inferred parameters specified. **E.** The relationship between participants age and cognitive ability. **F.** Main effect of ACME, signifying the integrity of the large-scale arousal circuit driven by each candidate arousal-driving region on cognitive ability. P-values are specified after FDR correction and the values below 0.05 are marked in red. **G.** Same as F but for interaction effect of ACME and age on cognitive ability. The main effect of age was not significant for any of these regions.

DISCUSSION

Prior research regarding the arousal system has mainly focused on the investigation of how the ascending pathway of this system shapes cognitive task performance. By contrast, the questions of whether and how higher-order cortical regions regulate the arousal state in a top-down manner has remained underexplored. Here we hypothesized that the quality of such top-down regulation in individual subjects is predictive of their cognitive abilities because each cognitive operation benefits from distinct level of arousal. The present work sheds light on the mechanisms underlying the cortical regulation of the tonic arousal state (inferred via pupil size): First, we identify select cortical regions that independently predict the arousal state (Figure 3A) – specifically, these regions are situated in posterior cingulate cortex (PCC), anterior ventral insula (AVI), superior parietal lobule (SPL), inferior parietal lobule (IPL), and anterior midcingulate cortex (AmCC); Second, we show that activity in these regions predicts large-scale cortical state modulation that is specifically mediated by the arousal system (Figure 3B); Finally, we show that the properties of one such identified arousal-regulating neural circuits – involving the PCC – predicts individual differences in an aggregate cognitive performance metric (Figure 4), in agreement with our hypothesis.

<u>Control of the arousal system by frontal and parietal cortical regions</u>

PCC and IPL are interconnected regions within the default mode network (DMN)[28]. While DMN activity has been traditionally considered task-irrelevant, recent research provides evidence that PCC is active in vast variety of tasks[29 30] – for example, visuospatial orientation and planning [31], orientation in time and inference of social relationships[32], subjective value representation[33,34], and emotional processing[35]. Further, anticipatory prestimulus activity in PCC mediates allocation of top-down spatial attention[36] and predicts subsequent insight during a problem solving task[37]. Previous work also suggests that a small

number of DMN regions, and PCC in particular, are recruited when a change of context is required[38,39]. According to our results, one plausible explanation of DMN involvement in such an overwhelming variety of tasks is that DMN regions have the capacity to regulate tonic arousal.

Our data suggests that bilateral PCC (POS1) and right IPL (PGs), despite being interconnected anatomically and functionally, show independent effects on the arousal state at rest (Figure 3A). This result is consistent with a previous human 3T fMRI study examining the interaction between cortical activity and the arousal state in 20 individuals[16]. In our study of 107 individuals with 7T fMRI, however, ventromedial prefrontal cortex (vmPFC), another major DMN hub, despite showing a positive correlation with arousal (Figure 2B), did not show a significant group-level independent effect (Figure 3A). Interestingly, we find that a region in anterior midcingulate cortex, which is situated in close proximity to vmPFC, does show an independent contribution to predicting the tonic arousal state. Such a discrepancy could be explained by lack of control for within-network functional connectivity in the previous study, although smaller sample size, lack of cortical parcellation and group-level differences between subjects recruited in the two studies are also likely to affect the results.

Sleep studies in humans show that PCC and IPL activity is positively correlated with wakefulness (highest during wakefulness and lowest during sleep)[40–42], similarly to LC tonic firing rate in animals, which is also highest in states of stress and lowest in sleep[2,20,43,44]. Interestingly, the correlation between PCC and mPFC that is normally observed in resting state disappears in deep stages of sleep[45]. These prior findings are consistent with the lack of independent contribution of mPFC to predicting the arousal state that we observe in our resting state data.

In addition to the DMN regions we discuss above, we have also identified five additional regions (Figure 3A) in frontal and parietal cortices that show properties of arousal regulation. While these five regions are not part of the DMN, they are situated in close proximity to the DMN. The properties of arousal-regulating circuits involving these regions did not predict individual differences in cognitive performance (Figure 4F), yet they may play role in behaviors that were not tested in the present study.

Right anterior ventral insula (rAVI), which is a part of FPN, has been mostly implicated in processing of affective experience[46–48] and is suggested to play a role in present-moment awareness and control of autonomic nervous system processes[49]. Our results are consistent with the idea that the rAVI recruits the brainstem arousal system to regulate tonic arousal state underlying the processing of emotions. One should note, however, that this is a cytoarchitectonicaly complex area only recently parcellated from anterior insula[50], which does not have a topological equivalent in macaques, mice or rats[47,51]. For these reasons, the previous studies may need be reevaluated and investigation of this area in humans is especially crucial. For example, the adjacent dorsal anterior insula area, belonging to CON, has been previously proposed to play a role in tonic alertness regulation during task performance[52] and therefore dedicated future experiments are needed to disentangle between the distinct components of emotion-related and emotion-neutral tonic arousal state regulation, along with recordings from both ventral and dorsal insula and LC.

Anterior midcingulate cortex (AmCC, a32pr) has been previously implicated in evaluating motivation, anticipating outcomes, recognizing reward values[53,54] as well as proactive prediction and monitoring of decision outcomes during social interactions[55]. Such involvement in proactive and lasting behavioral modulation is consistent with our findings of this area affecting tonic arousal. Further, while AmCC has no cytoarchitectonic equivalent in rats, mice, and macaques[56], rodent ACC is considered to be a close relative and anterograde tracing of rat ACC axons shows their close proximity to distal LC dendrites[57], which is also consistent with our findings.

Superior parietal lobule (SPL, 7am/7al) is an area that is involved in multimodal integrated visuo-spatial representation, egocentric body coding and attentional processes[58,59]. 7al belongs to the somatomotor network and shows greater activity in motor processing tasks as compared to 7am, which belongs to the CON[60].

In sum, all the eight cortical brain regions that we uncovered herein are clearly involved in a great diversity of cognitive tasks and are considered to be somewhat mysterious, multimodal, or integrative areas. Our findings suggest that these areas have indirect neuromodulatory properties, which may explain why they have such extensive functional profiles.

The role of top-down arousal regulation in general fluid intelligence

Humans can reason without reliance on previously acquired knowledge. This remarkable ability is termed "fluid" reasoning – a high-level cognitive process that extracts relational information from the environment and manipulates that information to arrive at a solution to a problem at hand. To date, no consensus theory has been established on how the brain implements this ability, which obstructs the development of techniques to improve it (e.g., via education) or prevent its decline (e.g., by eliminating harmful practices).

Fluid reasoning is often assessed using a variety of cognitive tasks – for example, sorting of abstract sensory stimuli according to a given dimension, such as shape or color[61,62], or completion of a series of geometric patterns[63], as well as tests of working and episodic memory. Processing speed and inhibitory control tasks are also used to simulate the demands of a dynamic external environment where prior knowledge cannot be utilized. The performance metrics in such seemingly disparate sets of tasks are correlated[64], which suggests a shared underlying neural mechanism.

Neuroscience research has identified multiple frontoparietal brain regions and their interaction playing a role in fluid reasoning[65,66], with mostly multiple demand, "task-positive" network[67,68] and lateral prefrontal cortex in particular [69,70] involved. It is not known what processes could drive such widespread network-level phenomena, but the involvement of noradrenergic modulation has been recently proposed [7]. Indeed, arousal states and neuromodulatory systems are known to drive large-scale brain activity and network reconfiguration[71–73]. The results presented herein expand these ideas as follows – the properties of the ascending neuromodulatory system alone do not appear to be sufficient to explain individual variability in cognitive performance, but the properties of the whole circuit, including the top-down cortical control of the arousal state, do predict cognition (Figure 4).

<u>Limitations</u>

In the present study the regions driving the arousal state were calculated at the group level. However, it is possible that individual brains develop distinct connectivity pathway to control the arousal system, which could not be detectable at the group level. More detailed anatomical studies are required to discern projections from cortex to LC in humans, and a future study would be required to test functional connectivity and behavioral relevance of such arousal regulating circuits in individual brains. Nonetheless, we employed statistics (subject as a random effect) that provided evidence that the reported results generalized across the individuals in this study, and that the results are likely to generalize to other subjects not included in this study.

In the present work, the arousal state has been estimated via pupil diameter, which, in addition to LC, is driven by other neuromodulatory systems, such as the cholinergic basal forebrain (BF-ACh)[73]. The BF-Ach system possesses general properties similar to LC-NE in the context of the present study hypothesis – that is, BF-ACh neurons branch extensively to cover the entirety of cortex[24], and the release of ACh in cortex also results in inhibition of spontaneous brain activity[74,75]. Little is known about cortical projections back to BF in humans, but animal research indicates influence of projections from prefrontal cortex[76]. For these reasons, future research is needed to determine whether cortical regions discovered herein as arousal-driver regions influence brain state via neuromodulatory systems beyond LC.

<u>Future directions</u>

One research trajectory that can be enriched by our findings is the study of how to improve human cognition and fluid reasoning in health and disease. For example, meditation is a form of mental training

often requiring practicing sustained focus on an object (such as breath) which leads to improvement of cognition and, intriguingly, such training specifically involves the brain regions discovered herein as arousal-regulating regions[77]. Multiple studies and their meta-analysis identified a meditation-supporting network of regions that includes superior parietal cortex (region 7a), right insula and DMN regions, PCC and IPL[78]. PCC activity is lower in experienced meditators during practice compared to matched controls and compared to a non-meditation-related active task[79,80]. Mindfulness mediation also causes structural changes in the brain, for example, gray matter thickness in left PCC is smaller in experienced meditators[81]. Meta-analysis of meditation-induced connectivity shows increase of functional connectivity between PCC and AmCC[82], another region that supports arousal control according to our data. These results are generally consistent with our findings of positive correlations between these regions' activity and arousal (Figure 3A) and the reports of stress reduction and maintenance of relaxed focus in experienced meditators. A future study is needed to determine whether meditation causally affects the large-scale arousal-related circuitry we have identified herein. Considering our finding of better cognitive performance with more negative ACME (Figure 4), a plausible hypothesis would be that meditation leads to reduction in ACME during resting state. Other options for targeting the same circuit would involve causal manipulation of the functional connections themselves, such as via invasive[83] or non-invasive[84] brain stimulation or via neurofeedback-based training[85–87].

Another important direction is to investigate the brain circuits we identified herein in neuropsychiatric disorders that involve abnormalities of the arousal system – such as Alzheimer's, Schizophrenia, mood disorders, ADHD, and PTSD[9,88,89]. While the typical therapeutic intervention so far entails NE regulation of brain state[90–95], the select higher-order cortical regions that we identified herein are likely also able to invoke modulation of brain state, and should be now considered as promising upstream regions for therapeutic interventions.

Acknowledgements:

We thank Takuya Ito for useful comments on initial research findings.

METHODS

fMRI data selection and preprocessing

We used the Human Connectome Project (HCP) 7 Tesla dataset acquired at the Center for Magnetic Resonance Research at the University of Minnesota. The detailed description of the dataset is widely available – here, we provide only succinct summary pertaining our study for the readers' convenience. 184 subjects were scanned, however, resting state data with concurrent eye-tracking were missing in 8 subjects. All subjects were generally healthy young adults between 22 and 36 years old (mean age = 29.4, standard deviation = 3.3). There were 106 females and 70 males. Resting state runs of 15 minutes (up to four per subject) were collected using gradient-echo-planar imaging (EPI) sequence with the following parameters: repetition time (TR) = 1000 ms, echo time (TE) = 22.2 ms, flip angle = 45 deg, field of view (FOV) = 208 × 208 mm, matrix = 130 × 130, spatial resolution = 1.6 mm3, number of slices = 85, multiband factor = 5, image acceleration factor (iPAT) = 2, partial Fourier sampling = 7/8, echo spacing = 0.64 ms, bandwidth = 1924 Hz/Px. The direction of phase encoding alternated between posterior-to-anterior (PA) and anterior-to-posterior (AP). During rest runs, subjects were instructed to keep their eyes open and maintain relaxed fixation on a projected bright crosshair on a dark background.

Out of 176 subjects with available data, we selected 296 sessions from 108 subjects that had high-quality eye tracking (see below selection criteria). We used "fix-denoised" data preprocessed by the HCP team (files named *_Atlas_MSMAll_hp2000_clean.dtseries.nii). Briefly, the preprocessing pipeline followed standard preprocessing procedure (motion correction, distortion correction, high-pass filtering, and

nonlinear alignment to MNI template space [96] plus regression of 24 framewise motion estimates (six rigid-body motion parameters and their derivatives and the squares of those) and regression of confound timeseries identified via independent components analysis [97,98]. The data was aligned using multimodal surface matching algorithm II (MSMAII), which provides markedly better cross-subject cortical alignment than does volume-based alignment [99].

Eye-tracking data selection and preprocessing

Resting state eye-tracking data were downloaded from the following HCP database directory: subj#/unprocessed/7T/rfMRI_REST*/LINKED_DATA/EYETRACKER/. Eye-tracking data in these directories were found only for 149 out of 184 subjects. In total eye-tracking data from 576 runs were downloaded (15 minutes each), 1- 4 runs per subject. The eye-tracking data were acquired at 500Hz sampling rate in 68 runs and 1000Hz in 508 runs. The recordings were monocular, where left-eye pupil size data were present in 561 runs, and right-eye data in 4 runs, whereas pupil size data were completely missing from 11 runs. Considering normal blink rate of up to 15 blinks per minute, and blink duration up to 0.5 s, we normally expect up to 12.5 % (0.5 s * 15 / 60 s) pupil size data missing from the recordings. In addition, pupil size data can be missing because of uninstructed eye closure, saccades, failure of pupil detection in eye-tracking software. We allowed additional 7.5% missing data from such causes and selected only runs with pupil size data available at more than 80% of time samples, resulting in 334 runs, (supplementary figure 1A-B for missing data % distribution across runs, and examples of raw data quality) for further analysis. In addition, runs with incomplete fMRI data acquired (TR count less than 900, according to the provided session summary csv files) were excluded. Thus, in total, 296 runs from 108 subjects were selected for further analysis.

For each individual run, missing pupil data periods along with +/-100 ms surrounding samples were interpolated using Piecewise Cubic Hermite Interpolating Polynomial (PCHIP), which uses monotonic cubic splines to find the value of new points. Next, pupil size samples matching each MR image acquisition window were averaged, the timecourse convolved with a hemodynamic response function (HRF) (supplementary figure 1C-D), and z-scored to create the arousal predictor.

Identification of arousal driver regions

We first constructed a network-specific linear mixed model for arousal predictor *Pupil*, as follows:

$$Pupil_{it} \sim \beta_0 + \sum_{k \in w} \beta_k X_{kit} + \sum_{k \in w} \gamma_{ki} X_{kit} + \epsilon_{1it} \quad (1)$$

Where X denotes brain activity in potential driver region k within one resting state network w, β represent fixed effects and γ random effects, i is the subject and t is time in TR units. The analysis was conducted separately for each hemisphere and included n = 108 participants, whereas each participant's dataset contained between 900 to 3600 time points, resulting in 265,500 total observations for each model variable. No network-specific model contained brain regions with variance inflation factor larger than 10, indicating acceptable multicollinearity. Only random slopes were included since brain activity was normalized for each participant to ensure standardized parameters estimates. To allow reliable model fit and ensure convergence, the timing of maximal cross-correlation between individual brain region's activity and pupil size was calculated, and the brain activity shifted in time assuring optimal alignment. Finally, the regions that showed significant fixed effects for each network were then submitted to a cross-network linear mixed model (same formula as above). This two-step procedure ensured acceptable computational complexity required for model convergence.

Mediation analysis

For each driver region and each network or subcortical region, we conducted a group-level mediation analysis using two linear mixed models:

$$Pupil_{it} \sim \beta_0 + \beta_1 X_{it} + \sum_k \beta_k Z_{kit} + \gamma_{0i} + \gamma_{1i} X_{it} + \sum_k \gamma_{2ki} Z_{kit} + \epsilon_{1it} \quad (2)$$

$$Y_{it} \sim \beta_2 + \beta_3 Pupil_{it} + \beta_4 X_{it} + \sum_k \beta_k Z_{kit} + \gamma_{2i} + \gamma_{3i} Pupil_{it} + \gamma_{4i} X_{it} + \sum_k \gamma_{5k} Z_{kit} + \epsilon_{2it} \quad (3)$$

Where X represents the driver region (identified according to eq. (1)) activity and Y represents the outcome network averaged activity for subject i at time t. Z represents activity of remaining driver regions within the same hemisphere. To calculate Y, the region-level brain activity was first shifted according to the time of strongest negative correlation with pupil size, and averaged across all regions. (As a result of this procedure, the trough of the correlation between the averaged brain activity and pupil size was centered at zero.) βs are fixed effects parameters (shared by all subjects), γ_i are random effects parameters for subject i. The mediation effect was calculated as ACME (Average Causal Mediation Effect), which equals the product of β_1 and β_3. The *p*-value of ACME was estimated via bootstrapping of 1000 simulations using the Statsmodels toolbox, which uses independent random sampling of exogenous and endogenous variables.

Cognitive ability scores

We used fluid cognition composite scores calculated from NIH toolbox Cognition Battery in conjunction with Penn matrices reasoning test scores to assess individual cognitive ability. The fluid cognition composite score is computed as an aggregate of behavioral metrics in the Dimensional Change Card Sort (DCCS) test, Flanker, Picture Sequence Memory, List Sorting, and Pattern Comparison measures. Briefly, in the DCCS test the participant is asked to match a series of picture pairs to a target picture according to stimulus dimensions that change across trials (color or shape) and is used to assess cognitive flexibility. In the Flanker test the participant is asked to focus on a particular stimulus while inhibiting attention to the stimuli flanking it—this test is used to assess inhibitory control and attention. The Picture Sequence Memory test assesses episodic memory—participants are shown pictures of objects and activities, and then asked to reproduce the sequence of pictures as it was presented to them. List Sorting is a working memory test, which requires participants to recall and sequence different visual and auditory stimuli. The Pattern Comparison test specifically targets the measurement of processing speed—the participants are requested to determine whether two stimuli are the same or not. To calculate the aggregate, the test results were first converted to normally distributed scores and then averaged across tests. More details on measures and their validity are available in [100,101]. We used age-unadjusted scores and opted for including age as a variable in the model because of the previously reported interaction between arousal dynamics and age . Fluid cognition composite scores were averaged with a performance metric (number of correct responses) from the Penn matrices reasoning test (both metrics z-scored prior to averaging). This test was originally designed as a simplified Raven's Standard Progressive Matrices test including only 24 items (unlike 60 in Raven's) and includes abstract geometric patterns to be completed via multiple choice options.

Analysis of individual differences in behavior

To examine individual differences in behavior, we first fit a mediation model for each subject as follow (analogously to a group-level model):

$$Pupil_t \sim \beta_0 + \beta_1 X_t + \sum_k \beta_k Z_{kt} + \epsilon_{1t} \quad (4)$$

$$Y_t \sim \beta_2 + \beta_3 Pupil_t + \beta_4 X_t + \sum_k \beta_k Z_{kt} + \epsilon_{2t} \quad (5)$$

Next, we use the product of β_1 and β_3 (that is, ACME) averaged across networks or subcortical regions to predict the behavioral variables. Because both fluid reasoning ability and arousal dynamics are affected by age, we also included age as a covariate in the analysis:

$$Behavior_i \sim S_0 + S_1 \beta_{1i} \beta_{3i} + S_2 age_i + S_3 \beta_{1i} \beta_{3i} * age + \epsilon_3 \quad (6)$$

Control models, included β_1 or β_3, and age:

$$Behavior_i \sim S'_0 + S'_1\beta_{1i} + S'_2 age_i + S'_3\,\beta_{1i} * age + \epsilon_3 \quad (7)$$

$$Behavior_i \sim S''_0 + S''_1\beta_{3i} + S''_2 age_i + S''_3\,\beta_{3i} * age + \epsilon_3 \quad (8)$$

Bibliography

1. McCormick, D. A., Nestvogel, D. B. & He, B. J. Neuromodulation of Brain State and Behavior. *Annual Review of Neuroscience* **43**, 391–415 (2020).
2. Berridge, C. W. & Waterhouse, B. D. The locus coeruleus-noradrenergic system: Modulation of behavioral state and state-dependent cognitive processes. *Brain Research Reviews* **42**, 33–84 (2003).
3. Aston-Jones, G. & Cohen, J. D. AN INTEGRATIVE THEORY OF LOCUS COERULEUS-NOREPINEPHRINE FUNCTION: Adaptive Gain and Optimal Performance. *Annual Review of Neuroscience* **28**, 403–450 (2005).
4. Podvalny, E., King, L. E. & He, B. J. Spectral signature and behavioral consequence of spontaneous shifts of pupil-linked arousal in human. *eLife* **10**, e68265 (2021).
5. van Kempen, J. *et al.* Behavioural and neural signatures of perceptual decision-making are modulated by pupil-linked arousal. *eLife* **8**, e42541 (2019).
6. Waschke, L., Tune, S. & Obleser, J. Local cortical desynchronization and pupil-linked arousal differentially shape brain states for optimal sensory performance. *eLife* **8**, e51501 (2019).
7. Tsukahara, J. S. & Engle, R. W. Fluid intelligence and the locus coeruleus–norepinephrine system. *Proceedings of the National Academy of Sciences* **118**, e2110630118 (2021).
8. Suler, J. R. Primary process thinking and creativity. *Psychological Bulletin* **88**, 144–165 (1980).
9. Yamamoto, K., Shinba, T. & Yoshii, M. Psychiatric symptoms of noradrenergic dysfunction: A pathophysiological view. *Psychiatry and Clinical Neurosciences* **68**, 1–20 (2014).

465 10. Breton-Provencher, V., Drummond, G. T. & Sur, M. Locus Coeruleus Norepinephrine in
466 Learned Behavior: Anatomical Modularity and Spatiotemporal Integration in Targets.
467 *Frontiers in Neural Circuits* **15**, 46 (2021).
468 11. Poe, G. R. *et al.* Locus coeruleus: a new look at the blue spot. *Nat Rev Neurosci* **21**, 644–659
469 (2020).
470 12. Ranjbar-Slamloo, Y. & Fazlali, Z. Dopamine and Noradrenaline in the Brain; Overlapping or
471 Dissociate Functions? *Frontiers in Molecular Neuroscience* **12**, (2020).
472 13. Szabadi, E. Functional neuroanatomy of the central noradrenergic system. *J*
473 *Psychopharmacol* **27**, 659–693 (2013).
474 14. Jodo, E., Chiang, C. & Aston-Jones, G. Potent excitatory influence of prefrontal cortex
475 activity on noradrenergic locus coeruleus neurons. *Neuroscience* **83**, 63–79 (1998).
476 15. Jodo, E. & Aston-Jones, G. Activation of locus coeruleus by prefrontal cortex is mediated by
477 excitatory amino acid inputs. *Brain Research* **768**, 327–332 (1997).
478 16. Yellin, D., Berkovich-Ohana, A. & Malach, R. Coupling between pupil fluctuations and
479 resting-state fMRI uncovers a slow build-up of antagonistic responses in the human cortex.
480 *NeuroImage* **106**, 414–427 (2015).
481 17. Waterhouse, B. D. & Navarra, R. L. The locus coeruleus-norepinephrine system and sensory
482 signal processing: A historical review and current perspectives. *Brain Research* **1709**, 1–15
483 (2019).
484 18. Armstrong-James, M. & Fox, K. Effects of ionophoresed noradrenaline on the spontaneous
485 activity of neurones in rat primary somatosensory cortex. *J Physiol* **335**, 427–447 (1983).
486 19. Aston-Jones, G., Segal, M. & Bloom, F. E. Brain aminergic axons exhibit marked variability
487 in conduction velocity. *Brain Research* **195**, 215–222 (1980).

20. Aston-Jones, G. & Bloom, F. E. Activity of norepinephrine-containing locus coeruleus neurons in behaving rats anticipates fluctuations in the sleep-waking cycle. *J. Neurosci.* **1**, 876–886 (1981).

21. Vazey, E. M., Moorman, D. E. & Aston-Jones, G. Phasic locus coeruleus activity regulates cortical encoding of salience information. *Proceedings of the National Academy of Sciences* **115**, E9439–E9448 (2018).

22. Servan-Schreiber, D., Printz, H. & Cohen, J. D. A network model of catecholamine effects: gain, signal-to-noise ratio, and behavior. *Science* **249**, 892–895 (1990).

23. Bassant, M. H., Ennouri, K. & Lamour, Y. Effects of iontophoretically applied monoamines on somatosensory cortical neurons of unanesthetized rats. *Neuroscience* **39**, 431–439 (1990).

24. van den Brink, R. L., Pfeffer, T. & Donner, T. H. Brainstem Modulation of Large-Scale Intrinsic Cortical Activity Correlations. *Frontiers in Human Neuroscience* **13**, 340 (2019).

25. Ji, J. L. *et al.* Mapping the human brain's cortical-subcortical functional network organization. (2018) doi:10.1101/206292.

26. Liu, K. Y. *et al.* Noradrenergic-dependent functions are associated with age-related locus coeruleus signal intensity differences. *Nat Commun* **11**, 1712 (2020).

27. Bugg, J. M., Zook, N. A., DeLosh, E. L., Davalos, D. B. & Davis, H. P. Age differences in fluid intelligence: Contributions of general slowing and frontal decline. *Brain and Cognition* **62**, 9–16 (2006).

28. Buckner, R. L., Andrews-Hanna, J. R. & Schacter, D. L. *The brain's default network: Anatomy, function, and relevance to disease*. *Annals of the New York Academy of Sciences* vol. 1124 (2008).

510 29. Pearson, J. M., Heilbronner, S. R., Barack, D. L., Hayden, B. Y. & Platt, M. L. Posterior
511 cingulate cortex: adapting behavior to a changing world. *Trends in Cognitive Sciences* **15**,
512 143–151 (2011).
513 30. Foster, B. L. *et al.* A tripartite view of the posterior cingulate cortex. *Nat Rev Neurosci* **24**,
514 173–189 (2023).
515 31. Vatansever, D., Manktelow, A., Sahakian, B. J., Menon, D. K. & Stamatakis, E. A. Default
516 Mode Network Engagement Beyond Self-Referential Internal Mentation. *Brain Connectivity*
517 **8**, 245–253 (2018).
518 32. Peer, M., Salomon, R., Goldberg, I., Blanke, O. & Arzy, S. Brain system for mental
519 orientation in space, time, and person. *Proceedings of the National Academy of Sciences* **112**,
520 11072–11077 (2015).
521 33. Kable, J. W. & Glimcher, P. W. The neural correlates of subjective value during
522 intertemporal choice. *Nature neuroscience* **10**, 1625–33 (2007).
523 34. Levy, I., Snell, J., Nelson, A. J., Rustichini, A. & Glimcher, P. W. Neural representation of
524 subjective value under risk and ambiguity. *J Neurophysiol* **103**, 1036–1047 (2010).
525 35. Maddock, R. J., Garrett, A. S. & Buonocore, M. H. Posterior cingulate cortex activation by
526 emotional words: fMRI evidence from a valence decision task. *Human Brain Mapping* **18**,
527 30–41 (2003).
528 36. Small, D. M. *et al.* The posterior cingulate and medial prefrontal cortex mediate the
529 anticipatory allocation of spatial attention. *NeuroImage* **18**, 633–641 (2003).
530 37. Kounios, J. *et al.* The Prepared Mind: Neural Activity Prior to Problem Presentation Predicts
531 Subsequent Solution by Sudden Insight. *Psychol Sci* **17**, 882–890 (2006).

532 38. Crittenden, B. M., Mitchell, D. J. & Duncan, J. Recruitment of the default mode network
533 during a demanding act of executive control. *eLife* **4**, e06481 (2015).
534 39. Smith, V., Mitchell, D. J. & Duncan, J. Role of the Default Mode Network in Cognitive
535 Transitions. *Cerebral Cortex* **28**, 3685–3696 (2018).
536 40. Maquet. Functional neuroimaging of normal human sleep by positron emission tomography.
537 *J Sleep Res* **9**, 207–231 (2000).
538 41. Sämann, P. G. *et al.* Development of the Brain's Default Mode Network from Wakefulness
539 to Slow Wave Sleep. *Cerebral Cortex* **21**, 2082–2093 (2011).
540 42. Vogt, B. A. & Laureys, S. Posterior cingulate, precuneal and retrosplenial cortices: cytology
541 and components of the neural network correlates of consciousness. in *Progress in Brain*
542 *Research* (ed. Laureys, S.) vol. 150 205–217 (Elsevier, 2005).
543 43. Rasmussen, K., Morilak, D. A. & Jacobs, B. L. Single unit activity of locus coeruleus
544 neurons in the freely moving cat: I. During naturalistic behaviors and in response to simple
545 and complex stimuli. *Brain Research* **371**, 324–334 (1986).
546 44. Takahashi, K., Kayama, Y., Lin, J. S. & Sakai, K. Locus coeruleus neuronal activity during
547 the sleep-waking cycle in mice. *Neuroscience* **169**, 1115–1126 (2010).
548 45. Horovitz, S. G. *et al.* Decoupling of the brain's default mode network during deep sleep.
549 *Proceedings of the National Academy of Sciences* **106**, 11376–11381 (2009).
550 46. Touroutoglou, A., Hollenbeck, M., Dickerson, B. C. & Feldman Barrett, L. Dissociable
551 large-scale networks anchored in the right anterior insula subserve affective experience and
552 attention. *NeuroImage* **60**, 1947–1958 (2012).
553 47. Uddin, L. Q. Salience processing and insular cortical function and dysfunction. *Nat Rev*
554 *Neurosci* **16**, 55–61 (2015).

555 48. Wager, T. D., Davidson, M. L., Hughes, B. L., Lindquist, M. A. & Ochsner, K. N.
556 Prefrontal-Subcortical Pathways Mediating Successful Emotion Regulation. *Neuron* **59**,
557 1037–1050 (2008).
558 49. Craig, A. D. B. How do you feel--now? The anterior insula and human awareness. *Nat Rev*
559 *Neurosci* **10**, 59–70 (2009).
560 50. Baker, C. M. *et al.* A Connectomic Atlas of the Human Cerebrum—Chapter 5: The Insula
561 and Opercular Cortex. *Oper Neurosurg (Hagerstown)* **15**, S175–S244 (2018).
562 51. Namkung, H., Kim, S.-H. & Sawa, A. The Insula: An Underestimated Brain Area in Clinical
563 Neuroscience, Psychiatry, and Neurology. *Trends in Neurosciences* **40**, 200–207 (2017).
564 52. Sadaghiani, S., Poline, J.-B., Kleinschmidt, A. & D'Esposito, M. Ongoing dynamics in large-
565 scale functional connectivity predict perception. *Proceedings of the National Academy of*
566 *Sciences of the United States of America* **112**, 8463–8 (2015).
567 53. Bush, G. *et al.* Dorsal anterior cingulate cortex: A role in reward-based decision making.
568 *PNAS* **99**, 523–528 (2002).
569 54. Bush, G., Luu, P. & Posner, M. I. Cognitive and emotional influences in anterior cingulate
570 cortex. *Trends in Cognitive Sciences* **4**, 215–222 (2000).
571 55. Apps, M., Lockwood, P. & Balsters, J. The role of the midcingulate cortex in monitoring
572 others' decisions. *Frontiers in Neuroscience* **7**, (2013).
573 56. Vogt, B. A. Midcingulate cortex: Structure, connections, homologies, functions and diseases.
574 *Journal of Chemical Neuroanatomy* **74**, 28–46 (2016).
575 57. Gompf, H. S. *et al.* Locus Ceruleus and Anterior Cingulate Cortex Sustain Wakefulness in a
576 Novel Environment. *J Neurosci* **30**, 14543–14551 (2010).

577 58. Scheperjans, F. *et al.* Probabilistic Maps, Morphometry, and Variability of Cytoarchitectonic
578 Areas in the Human Superior Parietal Cortex. *Cerebral Cortex* **18**, 2141–2157 (2008).
579 59. Wang, J. *et al.* Convergent functional architecture of the superior parietal lobule unraveled
580 with multimodal neuroimaging approaches. *Human Brain Mapping* **36**, 238–257 (2015).
581 60. Baker, C. M. *et al.* A Connectomic Atlas of the Human Cerebrum—Chapter 7: The Lateral
582 Parietal Lobe. *Oper Neurosurg (Hagerstown)* **15**, S295–S349 (2018).
583 61. Eling, P., Derckx, K. & Maes, R. On the historical and conceptual background of the
584 Wisconsin Card Sorting Test. *Brain and Cognition* **67**, 247–253 (2008).
585 62. Grant, D. A. & Berg, E. A behavioral analysis of degree of reinforcement and ease of
586 shifting to new responses in a Weigl-type card-sorting problem. *Journal of Experimental*
587 *Psychology* **38**, 404–411 (1948).
588 63. Raven, J. C. *Raven's progressive matrices (1938): sets A, B, C, D, E*. (Australian Council for
589 Educational Research, 1938).
590 64. Spearman, C. 'General Intelligence,' Objectively Determined and Measured. *The American*
591 *Journal of Psychology* **15**, 201–292 (1904).
592 65. Christoff, K. *et al.* Rostrolateral Prefrontal Cortex Involvement in Relational Integration
593 during Reasoning. *NeuroImage* **14**, 1136–1149 (2001).
594 66. Kroger, J. K. *et al.* Recruitment of Anterior Dorsolateral Prefrontal Cortex in Human
595 Reasoning: a Parametric Study of Relational Complexity. *Cerebral Cortex* **12**, 477–485
596 (2002).
597 67. Finn, E. S. *et al.* Functional connectome fingerprinting: identifying individuals using patterns
598 of brain connectivity. *Nat Neurosci* **18**, 1664–1671 (2015).

68. Woolgar, A., Duncan, J., Manes, F. & Fedorenko, E. Fluid intelligence is supported by the multiple-demand system not the language system. *Nat Hum Behav* **2**, 200–204 (2018).

69. Cole, M. W., Ito, T. & Braver, T. S. Lateral Prefrontal Cortex Contributes to Fluid Intelligence Through Multinetwork Connectivity. *Brain Connectivity* **5**, 497–504 (2015).

70. Cole, M. W., Yarkoni, T., Repovs, G., Anticevic, A. & Braver, T. S. Global Connectivity of Prefrontal Cortex Predicts Cognitive Control and Intelligence. *Journal of Neuroscience* **32**, 8988–8999 (2012).

71. Martin, C. G., He, B. J. & Chang, C. State-related neural influences on fMRI connectivity estimation. *NeuroImage* **244**, 118590 (2021).

72. Oyarzabal, E. A. *et al.* Chemogenetic stimulation of tonic locus coeruleus activity strengthens the default mode network. *Science Advances* **8**, eabm9898 (2022).

73. Shine, J. M. *et al.* Human cognition involves the dynamic integration of neural activity and neuromodulatory systems. *Nature Neuroscience* **22**, 289–296 (2019).

74. Shulz, D. E., Cohen, S., Haidarliu, S. & Ahissar, E. Differential Effects of Acetylcholine on Neuronal Activity and Interactions in the Auditory Cortex of the Guinea-pig. *European Journal of Neuroscience* **9**, 396–409 (1997).

75. Randić, M., Siminoff, R. & Straughan, D. W. Acetylcholine depression of cortical neurons. *Experimental Neurology* **9**, 236–242 (1964).

76. Zaborszky, L., Gaykema, R. P., Swanson, D. J. & Cullinan, W. E. Cortical input to the basal forebrain. *Neuroscience* **79**, 1051–1078 (1997).

77. Tang, Y.-Y., Hölzel, B. K. & Posner, M. I. The neuroscience of mindfulness meditation. *Nat Rev Neurosci* **16**, 213–225 (2015).

621 78. Tomasino, B., Fregona, S., Skrap, M. & Fabbro, F. Meditation-related activations are
622 modulated by the practices needed to obtain it and by the expertise: an ALE meta-analysis
623 study. *Frontiers in Human Neuroscience* **6**, (2013).
624 79. Brewer, J. A. *et al.* Meditation experience is associated with differences in default mode
625 network activity and connectivity. *Proceedings of the National Academy of Sciences* **108**,
626 20254–20259 (2011).
627 80. Garrison, K. A., Zeffiro, T. A., Scheinost, D., Constable, R. T. & Brewer, J. A. Meditation
628 leads to reduced default mode network activity beyond an active task. *Cogn Affect Behav*
629 *Neurosci* **15**, 712–720 (2015).
630 81. Berkovich-Ohana, A. *et al.* Studying the precuneus reveals structure–function–affect
631 correlation in long-term meditators. *Social Cognitive and Affective Neuroscience* **15**, 1203–
632 1216 (2020).
633 82. Rahrig, H. *et al.* Meta-analytic evidence that mindfulness training alters resting state default
634 mode network connectivity. *Sci Rep* **12**, 12260 (2022).
635 83. Sun, F. T. & Morrell, M. J. The RNS System: responsive cortical stimulation for the
636 treatment of refractory partial epilepsy. *Expert Review of Medical Devices* **11**, 563–572
637 (2014).
638 84. Sehm, B. *et al.* Dynamic modulation of intrinsic functional connectivity by transcranial
639 direct current stimulation. *Journal of Neurophysiology* **108**, 3253–3263 (2012).
640 85. Harmelech, T., Preminger, S., Wertman, E. & Malach, R. The Day-After Effect: Long Term,
641 Hebbian-Like Restructuring of Resting-State fMRI Patterns Induced by a Single Epoch of
642 Cortical Activation. *Journal of Neuroscience* **33**, 9488–9497 (2013).

643 86. Ramot, M. *et al.* Direct modulation of aberrant brain network connectivity through real-time
644 NeuroFeedback. *eLife* **6**, e28974 (2017).
645 87. Ramot, M., Grossman, S., Friedman, D. & Malach, R. Covert neurofeedback without
646 awareness shapes cortical network spontaneous connectivity. *Proc Natl Acad Sci USA* **113**,
647 E2413–E2420 (2016).
648 88. Friedman, J. I., Adler, D. N. & Davis, K. L. The role of norepinephrine in the
649 pathophysiology of cognitive disorders: potential applications to the treatment of cognitive
650 dysfunction in schizophrenia and Alzheimer's disease. *Biological Psychiatry* **46**, 1243–1252
651 (1999).
652 89. Ressler, K. J. & Nemeroff, C. B. Role of norepinephrine in the pathophysiology and
653 treatment of mood disorders. *Biological Psychiatry* **46**, 1219–1233 (1999).
654 90. Biederman, J. & Spencer, T. Attention-deficit/hyperactivity disorder (adhd) as a
655 noradrenergic disorder. *Biological Psychiatry* **46**, 1234–1242 (1999).
656 91. Campo, N. del, Chamberlain, S. R., Sahakian, B. J. & Robbins, T. W. The Roles of
657 Dopamine and Noradrenaline in the Pathophysiology and Treatment of Attention-
658 Deficit/Hyperactivity Disorder. *Biological Psychiatry* **69**, e145–e157 (2011).
659 92. Moret, C. & Briley, M. The importance of norepinephrine in depression. *Neuropsychiatr Dis*
660 *Treat* **7**, 9–13 (2011).
661 93. Morilak, D. A. *et al.* Role of brain norepinephrine in the behavioral response to stress.
662 *Progress in Neuro-Psychopharmacology and Biological Psychiatry* **29**, 1214–1224 (2005).
663 94. Nutt, D. J. The Role of Dopamine and Norepinephrine in Depression and Antidepressant
664 Treatment. *J Clin Psychiatry* **67**, 18664 (2006).

95. Southwick, S. M. *et al.* Role of norepinephrine in the pathophysiology and treatment of posttraumatic stress disorder. *Biological Psychiatry* **46**, 1192–1204 (1999).

96. Glasser, M. F. *et al.* The minimal preprocessing pipelines for the Human Connectome Project. *Neuroimage* **80**, 105–124 (2013).

97. Griffanti, L. *et al.* Hand classification of fMRI ICA noise components. *NeuroImage* (2017) doi:10.1016/j.neuroimage.2016.12.036.

98. Salimi-Khorshidi, G. *et al.* Automatic denoising of functional MRI data: combining independent component analysis and hierarchical fusion of classifiers. *Neuroimage* **90**, 449–468 (2014).

99. Coalson, T. S., Van Essen, D. C. & Glasser, M. F. The impact of traditional neuroimaging methods on the spatial localization of cortical areas. *Proceedings of the National Academy of Sciences* **115**, E6356–E6365 (2018).

100. Heaton, R. K. *et al.* Reliability and Validity of Composite Scores from the NIH Toolbox Cognition Battery in Adults. *Journal of the International Neuropsychological Society* **20**, 588–598 (2014).

101. Scott, E. P., Sorrell, A. & Benitez, A. Psychometric Properties of the NIH Toolbox Cognition Battery in Healthy Older Adults: Reliability, Validity, and Agreement with Standard Neuropsychological Tests. *Journal of the International Neuropsychological Society* **25**, 857–867 (2019).

Supplementary figures

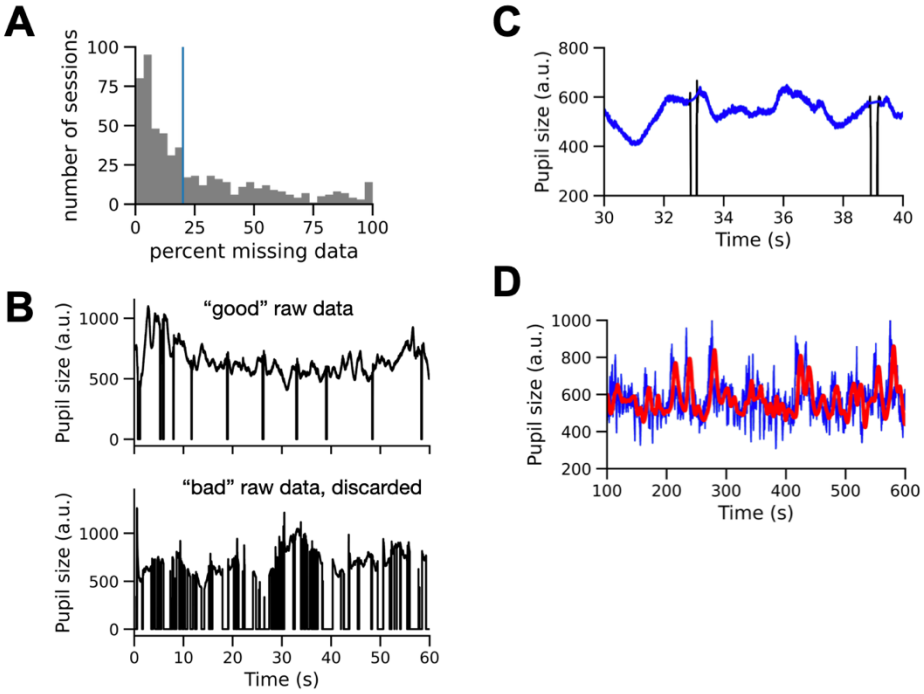

Supplementary figure 1. Eye-tracking data summary. A. Percent of time samples where the eye-tracking data were missing in each session. The blue vertical line indicates the cut-off of sessions that show above 20% missing data. **B.** Example of acceptable and unacceptable eye-tracking data quality. **C.** Example of blink correction procedure. **D.** Example of HRF convolved pupil size time course**.**

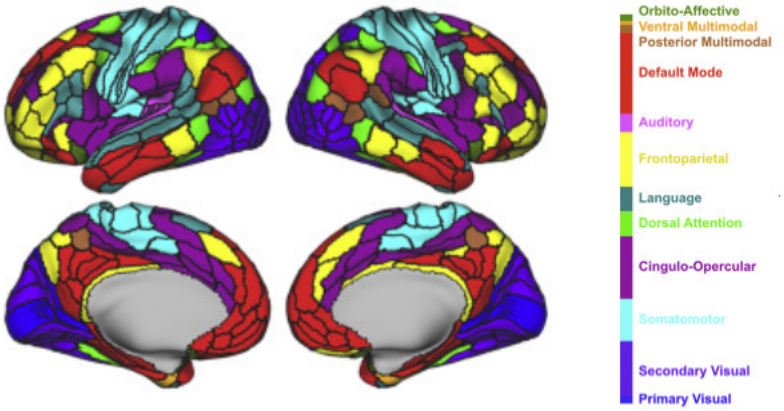

Supplementary figure 2. Cole-Anticevic partition. Figure reproduced with permission.